https://doi.org/10.1016/j.energy.2021.119798

Coupling properties and parametric optimization of a photovoltaic panel driven thermoelectric refrigerators system

Tianjun Liao[a, b], Qijiao He [a], Qidong Xu [a], Yawen Dai [a], Chun Cheng [a], Meng Ni[a]*

[a] *Department of Building and Real Estate, The Hong Kong Polytechnic University, Hung Hom, Kowloon, Hong Kong, China*

[b] *Department of Physics and Energy, Chongqing University of Technology, Chongqing 400054, China*

*Corresponding author. Email: meng.ni@polyu.edu.hk (M. Ni)

Abstract: The achievement of temperature and heat management by combining the photovoltaic (PV) power generation and semiconductor thermoelectric refrigerators (TERs) is significant for developing high performance and durable energy conversion systems. In this work, a new energy system combining PV with TERs is proposed and theoretically evaluated. At a given solar irradiance of 200 $W \cdot m^{-2}$, the electrical matching properties between two subsystems are studied and the TERs' operating regions are provided. The optimal efficiency of 13.9% is obtained by reasonably selecting the TERs' number and the structure parameters. Further, the effects of the solar irradiance on the optimal efficiency and the operating conditions are analyzed. The parametric optimal regions are identified to achieve a trade-off between the efficiency and the cooling heat flow rate. The impacts of the diode's ideal factor, the TERs' temperature span, and the PV panel's series internal resistance and shunt resistance on the system are revealed. The proposed model and the analysis may provide valuable strategies for designing PV-driven TERs.

Key words: PV panel; thermoelectric refrigerator; cooling heat flow; coupling properties; parametric optimization

Nomenclature

A area (m^2)
E_g silicon-based PV panel band-gap (eV)
G solar irradiance ($W \cdot m^{-2}$)
I electrical current (A)
I_0 reverse saturation current (A)
k_B Boltzmann constant ($J \cdot K^{-1}$)
K thermal conductance ($W \cdot K^{-1}$)
l length (m)
m ideal factor
N number of thermoelectric refrigerators
n_T number of p-n couples
n_{PV} number of solar cells in series
P power output (W)
q elementary positive charge (C)
$\dot{Q}$ heat flow (W)
R_s series internal resistance (Ω)
R_{sh} shunt resistance (Ω)
R_{TERs} internal resistance of TERs (Ω)
T temperature (K)
U heat transfer coefficient ($W \cdot m^{-2} \cdot K^{-1}$)
V voltage (V)
Z objective function (W)

Greek symbols

α Seebeck coefficient ($V \cdot K^{-1}$)
ρ electrical resistivity ($\Omega \cdot m$)
κ thermal conductivity ($W \cdot K^{-1} \cdot m^{-1}$)
σ Stefan-Boltzmann constant ($W \cdot K^{-4} \cdot m^{-2}$)
β structure parameter of TER (m)
μ short-circuit current coefficient ($A \cdot K^{-1}$)
η efficiency

Subscript

avg average
CP coupling point
E environment
H hot side
lb lower-bound
L cold side
n n- type semiconductor
max maximum
opt optimal
OC open-circuit
p p- type semiconductor
PV photovoltaic
ph photo-generation
Ref reference
SC short-circuit
SU start-up
ub upper-bound

Abbreviations

COP coefficient of performance
PV photovoltaic
TED thermoelectric device
TERs thermoelectric refrigerators

1. Introduction

Due to the increasingly energy crisis and environmental problems, the development and utilization of renewable energy have attracted tremendous attentions. Photovoltaic (PV) power generation technology is one of the key ways of solar energy utilization [1]. With the improvement and commercialization of silicon-based PV panel, the problems of electrical energy's storage and application need to be solved. Some researchers proposed solutions for storage the electrical energy by means of super-capacitors [2] and lithium-ion battery cells [3]. On the other hand, most of the solar energy is converted into irreversible thermal losses [4]. The finite-time heat transfer increases the temperature and decrease the photo-electric conversion efficiency. Consequently, it is of great importance for recovering the waste heat to achieve energy cascade utilization [5]. Researchers proposed methods of waste heat recovery and thermal management by attaching the thermoelectric devices (TEDs) [6] and thermoelectric refrigerators (TERs) [7] to the back-side of the PV panel. Yin *et. al.* [6] proposed a concentration spectrum splitting PV-TEG coupling system. The optimal cut-off wavelength at the highest efficiency was obtained. The effects of the TEG's thermal resistance and structure factor on the system were discussed. The results are significant for analyzing and optimizing the PV-TEG systems. Kane *et. al.* [7] attached a TER at the back side of PV panel for the purpose of thermal management. Considering the temperature dependence of material properties, a temperature based maximum power point tracking scheme was provided for operating TEM at optimal temperature of PV system. Najafi *et. al.* [8] utilized the PV panel's electricity to drive TER. Genetic algorithm was utilized to optimize the supplied electrical current for the TER, resulting the maximum power generation

in the PV panel. It has been demonstrated that the TER can assist the PV panel at a low-level temperature by using a reasonable amount of electricity. Although the decrease of temperature is achieved, the overall efficiency hasn't been improved due to the electrical energy consumption. As an important application, the electrical coupling models of solar cell driven TER systems were established [9, 10]. The effects of the electrical and the thermal parameters on cooling heat flow rate and efficiency were discussed. Cheng *et. al.* [11] utilized the solar cells driven TER system to cool the green building. Experimental results demonstrated that a 16.2 °C temperature difference between environment and indoor space can be produced. Although some literatures reported the PV driven TERs, the coupling properties and parametric optimization should be further studied.

In order to promote the application of PV panel in the field of refrigeration, we propose a model of PV panel driven TERs system in this work. The parameter coupling and matching characteristics between two subsystems are studied. The effects of solar irradiance, PV panel's diode ideal factor, and TERs' temperature span on the optimal performances and the operating conditions are discussed. The proposed model and the analysis can provide a theoretical basis for the design of solar refrigeration systems.

2. Model description of a PV panel driven TERs system

The schematic diagrams of a PV panel driven TERs system and an equivalent circuit of a silicon-based PV panel are illustrated in Fig. 1, where V_{PV} and I_{PV} denote the PV panel's output voltage and electrical current, I_{ph} and I_0 denote the PV panel's photo-generation and reverse saturation currents, R_{s} and R_{sh} are, respectively, the series internal resistance and shunt resistance, T_{L} and T_{H} stand for the temperatures of the cold and hot reservoirs,

U_{L} and U_{H} account for the heat transfer coefficients at the cold and hot sides [6], A_{L} and A_{H} mean the heat-transfer areas of the cold and hot junctions [12]. The PV panel converts sunlight into electrical energy based on the PV effect of the semiconductor p-n junction. Solar cells are connected in series and packaged to form a PV panel. In TERs, a thermocouple is composed of two types of doped semiconductor materials. As the system is in operation, the power generated in the PV panel is directly applied to driven the TERs. Meanwhile, the PV panel's electrical current enters into the TERs, which absorb heat $\dot{Q}_{\mathrm{L}}$ from the cold reservoir and simultaneously release heat $\dot{Q}_{\mathrm{H}}$ into the hot reservoir per unit time, resulting in temperature difference $\left(T_2 - T_1\right)$. Therefore, an inequality $\left(T_2 > T_{\mathrm{H}} > T_{\mathrm{L}} > T_1\right)$ should satisfy at the cooling process [12].

3. The overall efficiency of the coupling system

The overall efficiency η of the PV panel driven TERs system is defined as [9]

$$\eta = \frac{P_{\mathrm{PV}}}{GA_{\mathrm{PV}}} \frac{\dot{Q}_{\mathrm{L}}}{P_{\mathrm{TERs}}}, \tag{1}$$

where $P_{\mathrm{PV}} = V_{\mathrm{PV}} I_{\mathrm{PV}}$ and $P_{\mathrm{TERs}} = \dot{Q}_{\mathrm{H}} - \dot{Q}_{\mathrm{L}} = V_{\mathrm{TERs}} I_{\mathrm{TERs}}$ are, respectively, the output electricity of the PV panel and the input power of the TERs. V_{TERs} and I_{TERs} account for the TERs' input voltage and electrical current. G means the solar irradiance. $A_{\mathrm{PV}} = 1.6434\,\mathrm{m}^2$ describes the PV panel's front surface area [14]. As the circuit of the PV panel is directly connected to that of the TER, the electrical coupling conditions: $V_{\mathrm{PV}} = V_{\mathrm{TERs}}$, $I_{\mathrm{PV}} = I_{\mathrm{TERs}}$, and $P_{\mathrm{PV}} = P_{\mathrm{TERs}}$ can be satisfied [9]. The previous works demonstrated that a part of the solar energy absorbed by the PV panel is converted into electricity to drive the external load, and the remaining energy is parasitic inside the PV panel in the form of thermalization, Joule heat, and non-radiative recombination heat, which leads to the increase of temperature and the heat

transfer from the PV panel to the environment [15, 16]. As two objects are operated an infinitely small temperature difference, the heat transfer is reversible. However, the PV panel's operating temperature T_{PV} is higher than the normal environment temperature $T_{\mathrm{E}}=300\,\mathrm{K}$, the irreversible heat transfers is occurred. According to Newton's cooling law, black-body radiative law, and energy balance analysis, an equation can be given by [7, 13]

$$GA_{\mathrm{PV}}-P_{\mathrm{PV}}=U_{\mathrm{PV}}A\left(T_{\mathrm{PV}}-T_{\mathrm{E}}\right)+\sigma A\left(T_{\mathrm{PV}}^{4}-T_{\mathrm{E}}^{4}\right), \tag{2}$$

where $U_{\mathrm{PV}}=5\,\mathrm{W\cdot m^{-2}\cdot K^{-1}}$ denotes the convective heat transfer coefficient [17]. $\sigma=5.67\times10^{-8}\,\mathrm{W\cdot K^{-4}\cdot m^{-2}}$ is the Stefan-Boltzmann constant. $A=2A_{\mathrm{PV}}$ means the total area by considering the waste heat emissions of the top and the bottom surface of the PV panel.

As we assume that series internal resistance $R_{\mathrm{s}}\to0$ and shunt resistance $R_{\mathrm{sh}}\to\infty$ are generally considered in the equivalent diode circuit model, the relationship between the electrical current I_{PV} and the voltage V_{PV} of the PV panel is expressed as [18]

$$I_{\mathrm{PV}}=I_{\mathrm{ph}}-I_{0}\left[\exp\left(\frac{qV_{\mathrm{PV}}}{mk_{\mathrm{B}}T_{\mathrm{PV}}n_{\mathrm{PV}}}\right)-1\right], \tag{3}$$

where m is the diode's ideal factor. n_{PV} denotes the numbers of solar cells in series. $q=1.60\times10^{-19}\,\mathrm{C}$ is the elementary charge. $k_{\mathrm{B}}=1.38\times10^{-23}\,\mathrm{J\cdot K^{-1}}$ stands for the Boltzmann constant. The dependence of the photo-generation current I_{ph} on the optical, thermal, and electrical parameters is defined as [7]

$$I_{\mathrm{ph}}=\frac{G}{G_{\mathrm{Ref}}}\left[I_{\mathrm{ph,Ref}}+\mu\left(T_{\mathrm{PV}}-T_{\mathrm{Ref}}\right)\right], \tag{4}$$

where $G_{\mathrm{Ref}}=1000\,\mathrm{W\cdot m^{-2}}$ is the reference solar irradiance. $T_{\mathrm{Ref}}=298\,\mathrm{K}$ is the reference temperature. $I_{\mathrm{ph,Ref}}=9.43\,\mathrm{A}$ is the photo-generated current under reference solar irradiance

[14]. $\mu = 0.00047\,\mathrm{A}\cdot\mathrm{K}^{-1}$ is the short-circuit current temperature coefficient [14].

The diode reverse saturation current I_0 varying with the band-gap E_g and work temperature T_{PV} is given by [18]

$$\frac{I_0}{I_{0,\mathrm{Ref}}} = \left(\frac{T_{PV}}{T_{\mathrm{Ref}}}\right)^3 \exp\left[\frac{qE_g}{k_B}\left(\frac{1}{T_{\mathrm{Ref}}} - \frac{1}{T_{PV}}\right)\right], \tag{5}$$

where $I_{0,\mathrm{Ref}} = 1.25\,\mathrm{nA}$ is the reverse saturation current at reference temperature T_{Ref}. The PV panel's band-gap E_g as a function of the temperature T_{PV} is defined as [19, 20]

$$E_g = 1.17 - \frac{4.73\times10^{-4}T_{PV}^{\ 2}}{T_{PV}+636}. \tag{6}$$

For the convenience of discussion, we set a structure parameter $A_p/l_p = A_n/l_n = \beta$. The p- and n- doped Bi_2Te_3 based semiconductor elements are thermally in parallel and electrically connected in series to make a TER. Considering the Newton cooling law, the Joule law, and the Peltier effect within the TERs, the two heat flows $\dot{Q}_H$ and $\dot{Q}_L$ are given by [21-23]

$$\dot{Q}_H = \alpha T_2 I_{\mathrm{TERs}} - K\left(T_2 - T_1\right) + \frac{1}{2}I_{\mathrm{TERs}}^2 R_{\mathrm{TERs}} \tag{7}$$

and

$$\dot{Q}_L = \alpha T_1 I_{\mathrm{TERs}} - K\left(T_2 - T_1\right) - \frac{1}{2}I_{\mathrm{TERs}}^2 R_{\mathrm{TERs}}, \tag{8}$$

where $\alpha T_2 I_{\mathrm{TERs}}$ and $\alpha T_1 I_{\mathrm{TERs}}$ are the Peltier heat generated at the hot end and cold sides per unit time. $K\left(T_2 - T_1\right)$ denotes the Newton heat flow between the hot and cold sides. $\alpha = Nn_T\left(\alpha_p - \alpha_n\right)$, $K = Nn_T\beta\left(\kappa_p + \kappa_n\right)$, and $R_{\mathrm{TERs}} = Nn_T\beta^{-1}\left(\rho_p + \rho_n\right)$ are, respectively, the Seebeck coefficient, thermal conductance, and electrical resistance of TERs. N is the number of TERs in series. n_T means the number of p-n TE couples in a TER. A and l stand for the cross-sectional area and the length of the semiconductor element. ρ and κ represent the electrical resistivity and the thermal conductivity of a TER. The subscripts n

and p designate n- and p-type elements.

Commercial CP2–127–06 Melcor TER is applied in this work. A p-n TE couple's total Seebeck coefficient $\left(\alpha_{\mathrm{p}}-\alpha_{\mathrm{n}}\right)$, resistivity $\left(\rho_{\mathrm{p}}+\rho_{\mathrm{n}}\right)$, and thermal conductivity $\left(\kappa_{\mathrm{p}}+\kappa_{\mathrm{n}}\right)$ are calculated by using the formulas as [24, 25]

$$\alpha_{\mathrm{p}}-\alpha_{\mathrm{n}}=\left(22224.0+930.6\overline{T}-0.8805\overline{T}^{2}\right)\times10^{-9}, \tag{9}$$

$$\rho_{\mathrm{p}}+\rho_{\mathrm{n}}=\left(5112+163.4\overline{T}+0.6279\overline{T}^{2}\right)\times10^{-10}, \tag{10}$$

and

$$\kappa_{\mathrm{p}}+\kappa_{\mathrm{n}}=\left(62605.0-277.7\overline{T}+0.4131\overline{T}^{2}\right)\times10^{-4}, \tag{11}$$

where $\overline{T}=\left(T_1+T_2\right)/2$ is the cold and hot sides' mean temperature.

According to Newton's cooling law, the heat flows $\dot{Q}_{\mathrm{H}}$ and $\dot{Q}_{\mathrm{L}}$ can be expressed as [24]

$$\dot{Q}_{\mathrm{H}} = U_H A_H (T_2 - T_H) \tag{12}$$

and

$$\dot{Q}_{\mathrm{L}} = U_L A_L (T_L - T_1), \tag{13}$$

where $A_{\mathrm{H}}/N=A_{\mathrm{L}}/N=3.6\times10^{-3}\ \mathrm{m}^2$.

According to Eqs. (7) and (8), the input power P_{TERs} of the TERs can be obtained as

$$P_{\mathrm{TERs}}=\dot{Q}_{\mathrm{H}}-\dot{Q}_{\mathrm{L}}=\alpha\left(T_2-T_1\right)I_{\mathrm{TERs}}+I_{\mathrm{TERs}}^{2}R_{\mathrm{TERs}}, \tag{14}$$

where $\alpha\left(T_2-T_1\right)I_{\mathrm{TERs}}$ represents the electrical work that overcomes the thermoelectric potential. $I_{\mathrm{TERs}}^{2}R_{\mathrm{TERs}}$ denotes the PV panel's power consumption due to the TERs' internal resistance R_{TERs}.

Thus, the input voltage V_{TERs} of the TERs is derived as

$$V_{TER} = P_{TER}/I_{TER} = N\alpha\ (T_1-T_2) + NI_{TER}R_{TER}, \tag{15}$$

4. Coupling properties and parametric optimization

By using Eqs. (2)-(6), the dependence of the operating temperature T_{PV} on the voltage V_{PV} can be numerically determined for given related parameters. Inserting T_{PV} into Eq. (3), the curve of the electrical current I_{PV} as a function of the voltage V_{PV} can be generated, as shown in Fig. 2(a). Combining Eqs. (7)-(13), the variations of the temperatures T_1 and T_2 with the electrical current I_{TERs} can be obtained, as displayed in Fig. 2(b). Inserting T_1 and T_2 into Eqs. (9)-(11) and (15), the relationship between I_{TERs} and V_{TERs} can be derived, as depicted in Fig. 2(a). It is observed from Fig. 2(a) that I_{TERs} monotonically increases of V_{TERs}. We can determine a coupling point $(V_{\mathrm{CP}}, I_{\mathrm{CP}})$ in the two voltage-current characteristics curves of the TERs and the PV panel as $V_{\mathrm{PV}} = V_{\mathrm{TERs}} = V_{\mathrm{CP}} = 29.3\,\mathrm{V}$ and $I_{\mathrm{PV}} = I_{\mathrm{TERs}} = I_{\mathrm{CP}} = 1.55\,\mathrm{A}$. Only when the system is operated at the coupling point, the cooling process can be achieved. Fig. 2(b) shows that two temperatures $T_1 = T_{1,\mathrm{CP}} = 287\,\mathrm{K}$ and $T_2 = T_{2,\mathrm{CP}} = 315\,\mathrm{K}$ are obtained as $V_{\mathrm{TERs}} = V_{\mathrm{CP}}$. The case $\dot{Q}_{\mathrm{L}} = 0$ can be achieved by adjusting the input voltage V_{TERs}. The result $T_1 = T_{\mathrm{L}}$ is occurred based on Eq. (13). The voltage under the condition $\dot{Q}_{\mathrm{L}} = 0$ is denoted as start-up voltage V_{SU}. Fig. 2(b) shows that T_2 is close to T_{H} under the condition of $V_{\mathrm{TERs}} = V_{\mathrm{SU}}$. When the voltage V_{TERs} locates in the region of $V_{\mathrm{TERs}} < V_{\mathrm{SU}}$, the temperatures T_1 and T_2 locate in the regions of $T_1 > T_{\mathrm{L}}$ and $T_2 < T_{\mathrm{H}}$. In the above regions, the purpose of the refrigeration process isn't achieved, while the TERs can work as a heat pump. On the other hand, the PV panel's maximum output voltage is equal to the open-circuit voltage V_{OC}. Thus, the voltage V_{TERs} shouldn't operate in the region of $V_{\mathrm{TERs}} \geq V_{\mathrm{OC}}$. Thus, the voltage V_{TERs} should locate in the region

$$V_{\mathrm{SU}} < V_{\mathrm{TERs}} < V_{\mathrm{OC}}. \tag{16}$$

As set $V_{\mathrm{TERs}} = V_{\mathrm{OC}}$, a lower-bound temperature $T_{1,\mathrm{lb}}$ and a upper-bound temperature $T_{2,\mathrm{ub}}$

can be determined. Based on the in-equation (16), the operating regions of the temperatures T_1 and T_2 should be situated in:

$$T_{\mathrm{L}} > T_1 > T_{1,\mathrm{lb}} \tag{17}$$

and

$$T_{2,\mathrm{ub}} > T_2 > T_{\mathrm{H}}. \tag{18}$$

Inserting $T_{1,\mathrm{CP}}$ into Eq. (13), the cooling heat flow rate $\dot{Q}_{\mathrm{L}}$ can be computed. Further, substituting $\dot{Q}_{\mathrm{L}}$ in Eq. (1), the energy conversion efficiency $\eta = 13.9\%$. As we set $U_{\mathrm{H}} \to \infty$ and $U_{\mathrm{L}} \to \infty$, infinitely small temperature differences are occurred, i.e., $T_1 - T_{\mathrm{L}} \to 0$ and $T_2 - T_{\mathrm{H}} \to 0$. Under the reversible heat transfer conditions, the system's efficiency $\eta = 20.9\%$ and the coupling parameters $V_{\mathrm{CP}} = 28.7\,\mathrm{V}$ and $I_{\mathrm{CP}} = 1.66\,\mathrm{A}$ can be obtained. Making comparisons between the non-ideal and the ideal cases, one can find that the impacts of the irreversible heat transfer losses on the efficiency are obviously. We should enhance the system' efficiency by reducing heat transfer losses at the boundaries, e.g., selecting material with high heat transfer coefficient. For a given solar irradiance G, we can adjust the parameters β and N to make system present high performances. In next section, the effects of β and N on the system's coupling properties will be discussed.

The variations of the coupling voltage V_{CP}, the coupling current I_{CP}, the cold-side's coupling temperature $T_{1,\mathrm{CP}}$, the hot-side's coupling temperature $T_{2,\mathrm{CP}}$, and the efficiency η with N and β are depicted in Fig. 3. Fig. 3(a) shows that the coupling voltage V_{CP} monotonically increases with N as β is fixed, because increasing the number of TERs leads that we should increase the voltage V_{CP} to achieve the cooling process, and thus, V_{CP} increases. Fig. 3(b) shows that the voltage V_{CP} monotonically decreases with β for given

N, because the decrease of internal resistance R_{TERs} with structure parameter β causes that only decreasing the voltage V_{CP} can achieve the cooling process, and thus, V_{CP} decreases. The two sub-systems' current-voltage properties and the variations of V_{CP} with N and β determine the dependences of the V_{CP} on N and β, as demonstrated in Fig. 3(b). Fig. 3(c) shows that the temperature $T_{1,\mathrm{CP}}$ first decreases and then increases as β is increased, and thus, there exists a minimum value of $T_{1,\mathrm{CP}}$. Fig. 3(d) displays that the temperature $T_{2,\mathrm{CP}}$ is a monotonically decreasing function of N, while it first increases and then decreases as β is increased. Fig. 3(e) reveals that an optimal efficiency $\eta_{\mathrm{opt}}=14.4\%$ and the corresponding conditions $\beta_{\mathrm{opt}}=1.21$ and $N_{\mathrm{opt}}=5$ can be determined. Based on the values β_{opt} and N_{opt}, the optimal values $V_{\mathrm{opt}}=28.1\mathrm{V}$ and $I_{\mathrm{opt}}=1.75\mathrm{A}$ of V_{CP} and I_{CP} can be calculated. Therefore, the results reveal that selecting optimal values V_{opt}, I_{opt}, β_{opt}, and N_{opt} can make the coupled system present high performance. Based on the optimal efficiency η_{opt} and Eq. (1), the optimal cooling heat flow $\dot{Q}_{\mathrm{L,opt}}$ is determined as

$$\dot{Q}_{\mathrm{L,opt}}=\eta_{\mathrm{opt}}\left(GA_{\mathrm{PV}}\right). \tag{19}$$

The variations of η_{opt}, $\dot{Q}_{\mathrm{L,opt}}$, N_{opt}, V_{opt}, and I_{opt} with the solar irradiance G are shown in Fig. 4. Fig. 4(a) presents that the optimized efficiency η_{opt} attains a maximum value $\eta_{\max}=20.0\%$ at G_{η}, while there exists the positive correlation between $\dot{Q}_{\mathrm{L,opt}}$ and G. It is seen from Fig. 4(a) that $\dot{Q}_{\mathrm{L,opt}}$ is negligibly in the region of $G<G_{\eta}$. In order to discuss the parametric optimal selection of G, an objective function $Z=\eta_{\mathrm{opt}}\dot{Q}_{\mathrm{L,opt}}$ is introduced. The curve of Z varying with G is depicted in Fig. 4(b). Fig. 4(b) shows that Z attains a maximum value $Z_{\max}$ at G_Z. In the region of $G>G_Z$, the efficiency η_{opt} decrease as the incident solar irradiance G increases. Only the solar irradiance G locates

in the region of

$$G_\eta \le G \le G_Z , \tag{20}$$

we can make trade-off between η_{opt} and $\dot{Q}_{\text{L,opt}}$ to present high performances.

Fig. 4(c) shows that the structure parameter β_{opt} monotonically increases with increase in solar irradiance G. Based on in-equation (20), the optimal region of β is determined as

$$\beta_{\text{lb}} \le \beta \le \beta_{\text{ub}} , \tag{21}$$

where β_{lb} is a lower-bound value at G_η. β_{ub} is an upper-bound value at G_Z.

Fig. 4(c) shows that the two subsystems can be matched when the TERs' number N_{opt} keeps at a constant in certain region. The intrinsic regime is revealed as follows. As we further increase N, the result occurred $V_{\text{SU}} > V_{\text{OC}}$ leads that the PV panel can not drive the TERs. As we further decrease N, the coupling point is not close to the maximum power point of the PV panel. As a result, the phenomenon is caused by optimization and matching. Based on in-equation (20), the upper value $N_{\text{ub}} = 6$ and the lower-bound value $N_{\text{lb}} = 5$ are obtained. The results indicate that two values of the TERs' number N_{opt} can be chosen to optimally design the system. Furthermore, the problem of matching number of solar cells and TERs are solved. Fig. 4(d) shows that V_{opt} and I_{opt} monotonically increases with increase in solar irradiance G. Due to the increase of V_{opt} and I_{opt}, the optimal structure parameter β_{opt} should be increased to meet Eq. (15). Due to the optimal region of G, the optimal operating regions of V_{CP} and I_{CP} can be determined as

$$V_{\text{lb}} \le V_{\text{TERs}} \le V_{\text{ub}} \tag{22}$$

and

$$I_{\text{lb}} \le I_{\text{TERs}} \le I_{\text{ub}} . \tag{23}$$

It is observed from Fig. 4(d) that the optimal current $I_{\rm opt}$ is too much small in the region of $G \le G_\eta$, which leads that the TERs absorb small heat flow $\dot{Q}_{\rm L}$ from the cold reservoir, and thus, $\dot{Q}_{\rm L,opt}$ is negligibly, as verified in Fig. 4(a).

The effects of the diode ideal factor m and the hot reservoir's temperature $T_{\rm H}$ on the system's performances are revealed in Tables 1 and 2. The results in Tables 1 and 2 shows that the increase of m and the decrease of $T_{\rm H}$ lead to the enhancement of system performance. The ideal factor m influences the PV panel's electrical properties, e.g., the open-circuit voltage $V_{\rm OC}$

$$V_{\rm OC} = \frac{m k_{\rm B} T_{\rm PV} n_{\rm PV}}{q} \ln\left[\frac{I_{\rm ph}}{I_0} + 1\right]. \tag{24}$$

The positive relation between $V_{\rm OC}$ and m changes the voltage-current characteristics resulting the variation of coupling point $(V_{\rm CP}, I_{\rm CP})$ with m, and thus, the performances of the system are adjusted accordingly.

The decrease of $T_{\rm H}$ is accompanied by decrease of temperature span $(T_{\rm H} - T_{\rm L})$. Because the TERs' coefficient of performance $\dot{Q}_{\rm L}/P_{\rm TERs}$ is bounded by the Carnot limit, i.e.,

$$\frac{\dot{Q}_{\rm L}}{P_{\rm TERs}} \le \frac{T_{\rm L}}{T_{\rm H} - T_{\rm L}}. \tag{25}$$

Therefore, the improvement of the TERs' $\dot{Q}_{\rm L}/P_{\rm TERs}$ enhances the system's overall efficiency. Generally, the series internal resistance $R_{\rm s}$ and shunt resistance $R_{\rm sh}$ meet $R_{\rm s} \ne 0$ and $R_{\rm sh} \ne \infty$. Thus, Eq. (1) should be rewritten as [25]:

$$I_{\rm PV} = I_{\rm ph} - I_0 \left\{ \exp\left[\frac{q(I_{\rm PV} R_{\rm s} + V_{\rm PV})}{k_{\rm B} T_{\rm PV}}\right] - 1 \right\} - \frac{V_{\rm PV} + I_{\rm PV} R_{\rm s}}{R_{\rm sh}}. \tag{26}$$

For given $R_{\rm s}$ and $R_{\rm sh}$, Table 3 list the parametric values at the maximum efficiency $\eta_{\max}$ and the maximum objective function $Z_{\max}$, which are helpful for the parametric choices of

actual systems.

4. Conclusions

We have conceptually established and theoretically studied a model of the PV panel driven TERs system. Through the analysis of the coupling characteristics of the subsystem, the following research results are obtained.

(1) Using the parameters selections in Fig. 2, the efficiency $\eta = 13.9\%$ and the operating conditions $T_{1,\mathrm{CP}} = 287\,\mathrm{K}$, $T_{2,\mathrm{CP}} = 315\,\mathrm{K}$, $V_{\mathrm{CP}} = 29.3\,\mathrm{V}$, and $I_{\mathrm{CP}} = 1.55\,\mathrm{A}$ of the non-ideal irreversible TERs system are obtained. Ignoring the TERs' boundary heat transfers, we can obtain the ideal system's efficiency $\eta = 20.9\%$ at $V_{\mathrm{CP}} = 28.7\,\mathrm{V}$ and $I_{\mathrm{CP}} = 1.66\,\mathrm{A}$.

(2) According to optimize the number N and the structure parameter β of the TERs, the optimal efficiency $\eta_{\mathrm{opt}} = 14.4\%$ and the corresponding conditions $\beta_{\mathrm{opt}} = 1.21$, $N_{\mathrm{opt}} = 5$, $V_{\mathrm{opt}} = 28.1\,\mathrm{V}$, and $I_{\mathrm{opt}} = 1.75\,\mathrm{A}$ are achieved.

(3) Through the analysis of the effects of the solar irradiance G on the system's optimal performances, a maximum efficiency $\eta_{\max} = 20.0\%$ and the positive correlation between $Q_{\mathrm{L,opt}}$ and G are found.

(4) The impacts of the diode's ideal factor m, the hot reservoir's temperature T_{H}, and internal resistance R_{s} and shunt resistance R_{sh} on the system are revealed. Increasing m and decreasing T_{H} can improve the system's performance. Considering the non-ideal PV circuit model, the performances of the system are reduced relatively.

The theoretical works proven that the structure parameter of the TERs could be optimized to obtain the maximum efficiency [9]. The results are consistent with the analysis in the present work. The previous experimental work demonstrated that performance of the system

is strongly dependent on solar irradiance and temperature difference of hot and cold sides for the TER [10]. The cold reservoir's temperature could maintain the temperature in the refrigerator at 5～10 °C, and have a coefficient of performance (COP) about 0.30. The recent work demonstrated that the cold reservoir's temperature could reach of about 10 °C, while the hot reservoir's temperature was about 40 °C, resulting a higher COP of about 0.61 [26]. Set $T_{\mathrm{L}}=283\mathrm{K}$ and $T_{\mathrm{H}}=313\mathrm{K}$, the TER's highest COP and the PV-TER system's maximum efficiency can, respectively, reach 0.55 and 11% in this work, one can find that the COP is close to that in the Ref. [26].

The proposed model and the analysis provide valuable strategies for solving the parametric design problems between the TERs and the external power devices. Especially, the continuous efficiency enhancement of the perovskite solar cells will further promote the development of solar energy driven TERs.

Acknowledgements

This work has been supported by the Chongqing Research Program of Basic Research and Frontier Technology (cstc2020jcyj-msxmX0001), the Science and Technology Research Program of Chongqing Municipal Education Commission (Grant No. KJQN201901144) and Scientific Research Foundation of Chongqing University of Technology (Grant No. 2019ZD22), People's Republic of China. M. NI also thanks the financial support by Hong Kong Polytechnic University (Project ID: P0014036, account: G-YW3T).

References

[1] Nayak PK, Mahek S, Snaith HJ, Cahen D. Photovoltaic solar cell technologies: analysing the state of the art. Nat. Rev. Mater. 2019; 4: 269–285.

[2] Lechene BP, Clerc R, Arias AC. Theoretical analysis and characterization of the energy conversion and storage efficiency of photo-supercapacitors. Solar Energy Materials & Solar Cells 2017; 172: 202–212.

[3] Joos S, Weishar B, Bessler WG. Passive hybridization of a photovoltaic module with lithium-ion battery cells: A model-based analysis. J. Power Sources 2017; 348: 201–211.

[4] Pourkiaei SM, Ahmadi MH, Sadeghzadeh M, Moosavi S, Pourfayaz F, Chen L, Yazdi MAP, Kumar P. Thermoelectric cooler and thermoelectric generator devices: a review of present and potential applications, modeling and materials. Energy 2019; 186: 115849.

[5] Li G, Shittu S, Zhao X, Ma X. Preliminary experiment on a novel photovoltaic-thermoelectric system in summer. Energy 2019; 188: 116041.

[6] Yin E, Li Q, Xuan Y. A novel optimal design method for concentration spectrum splitting photovoltaic–thermoelectric hybrid system. Energy 2018; 163: 519–532.

[7] Kane A, Verma V, Singh B. Optimization of thermoelectric cooling technology for an active cooling of photovoltaic panel. Renewable & Sustainable Energy Reviews 2017; 75: 1295–1305.

[8] Najafi H, Woodbury KA. Optimization of a cooling system based on Peltier effect for photovoltaic cells. Solar Energy, 2013; 91: 152–160.

[9] Su S, Chen X, Wang J, Chen J. Performance evaluation and parametric optimum design of a thermoelectric refrigerator driven by a dye-sensitized solar cell. Int. J. Refrigeration 2015; 60: 62–69.

[10] Dai YJ, Wang RZ, Ni L. Experimental investigation and analysis on a thermoelectric refrigerator driven by solar cells. Solar Energy Materials and Solar Cells 2003; 77: 377–391.

[11] Cheng TC, Cheng C, Huang ZZ, Liao GC. Development of an energy-saving module via combination of solar cells and thermoelectric coolers for green building applications. Energy 2011; 36(1): 133–140.

[12] Pan Y, Lin B, Chen J. Performance analysis and parametric optimal design of an irreversible multi-couple thermoelectric refrigerator under various operating conditions. Appl. Energy 2007; 84(9): 882–892.

[13] Al-Nimr M A, Mugdad B. A hybrid absorption/thermo-electric cooling system driven by

a concentrated photovoltaic/thermal unit. Sustainable Energy Technologies and Assessments 2020; 40: 100769.

[14]https://www.wholesalesolar.com/1524436/suniva/solar-panels/suniva-opt285-60-4-100-silver-mono-solar-panel.

[15] Shen L, Li Z, Ma T. Analysis of the power loss and quantification of the energy distribution in PV module. Appl. Energy 2020; 260: 114333.

[16] Shang A, Li X Photovoltaic devices: opto-electro-thermal physics and modeling. Advanced Materials 2017; 29: 1603492.

[17] Ordonez-Miranda J, Ezzahri Y, Drevillon J, Joulain K. Transistorlike device for heating and cooling based on the thermal hysteresis of VO_2. Phys. Rev. Appl. 2016; 6: 054003.

[18] Liao T, Lin B, Yang Z. Performance characteristics of a low concentrated photovoltaic-thermoelectric hybrid power generation device. Int. J. Therm. Sci. 2014; 77: 158–164.

[19] Liao T, Xiao J, Tao C. Optimal design of a solar cell-driven electroluminescent refrigerator. J. Photon. Energy, 2020, 10(4): 044502.

[20] Varpula A, Prunnila M. Diffusion-emission theory of photon enhanced thermionic emission solar energy harvesters. J. Appl. Phys. 2012; 112(4): 044506.

[21] Zhao Q, Zhang H, Hu Z, Hou S. Achieving a broad-spectrum photovoltaic system by hybridizing a two-stage thermoelectric generator. Energy Convers. Manage. 2020; 211: 112778.

[22] Kishore RA, Nozariasbmarz A, Poudel B, Sanghadasa M, Priya S, Ultra-high performance wearable thermoelectric coolers with less materials, Nat. Commun. 2019; 10: 1765.

[23] Yin E, Li Q, Xuan Y. One-day performance evaluation of photovoltaic-thermoelectric hybrid system. Energy 2018; 143: 337–346.

[24] Lin J, Liao T, Lin B. Performance analysis and load matching of a photovoltaic–thermoelectric hybrid system. Energy Convers. Manage. 2015; 105: 891–899.

[25] Liao T, He Q, Xu Q, Dai Y, Cheng C, Ni M. Performance evaluation and optimization of a perovskite solar cell-thermoelectric generator hybrid system. Energy 2020; 201: 117665.

[26] Rahman S M A, Hachicha A A, Ghenai C, Saidur R, Said Z. Performance and life cycle analysis of a novel portable solar thermoelectric refrigerator. Case Studies in Thermal Engineering, 2020; 19: 100599.

List of Figures and Tables

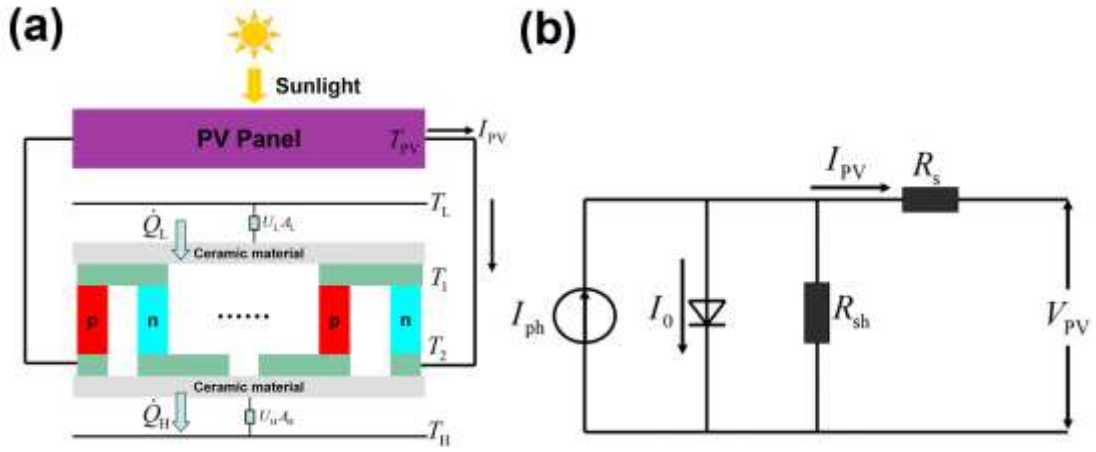

Fig. 1. (a) The schematic diagram of a PV-TERs system and (b) the equivalent circuit of a PV panel.

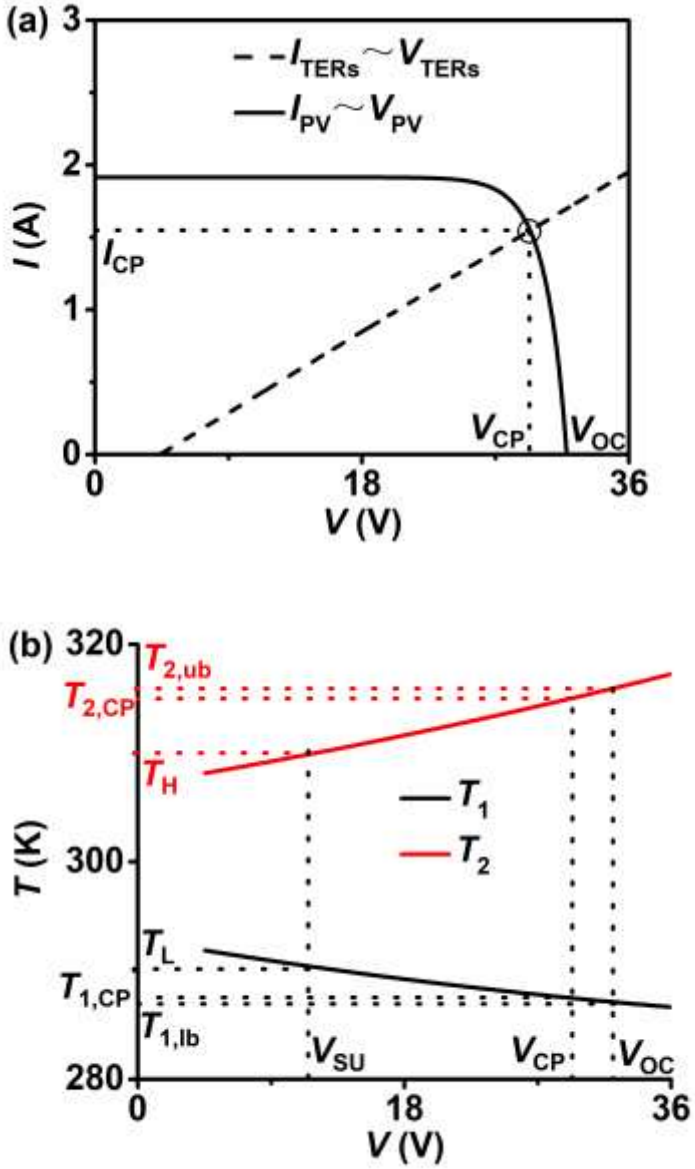

Fig. 2. (a) The current-voltage characteristics curves of the PV and the TERs and (b) the cold-side's temperature T_1 and hot-side's temperature T_2 of the TERs varying with the voltage V, where the parameters $G = 200\,\mathrm{W\cdot m^{-2}}$, $T_\mathrm{L} = 290\,\mathrm{K}$, $T_\mathrm{H} = 310\,\mathrm{K}$, $m = 1$, $U_\mathrm{H} = U_\mathrm{L} = 1000\,\mathrm{W\cdot m^{-2}\cdot K^{-1}}$, $n_\mathrm{T} = 127$, $n_\mathrm{PV} = 60$, $N = 5$, and $\beta = 1.00\times10^{-3}\,\mathrm{m}$ are selected.

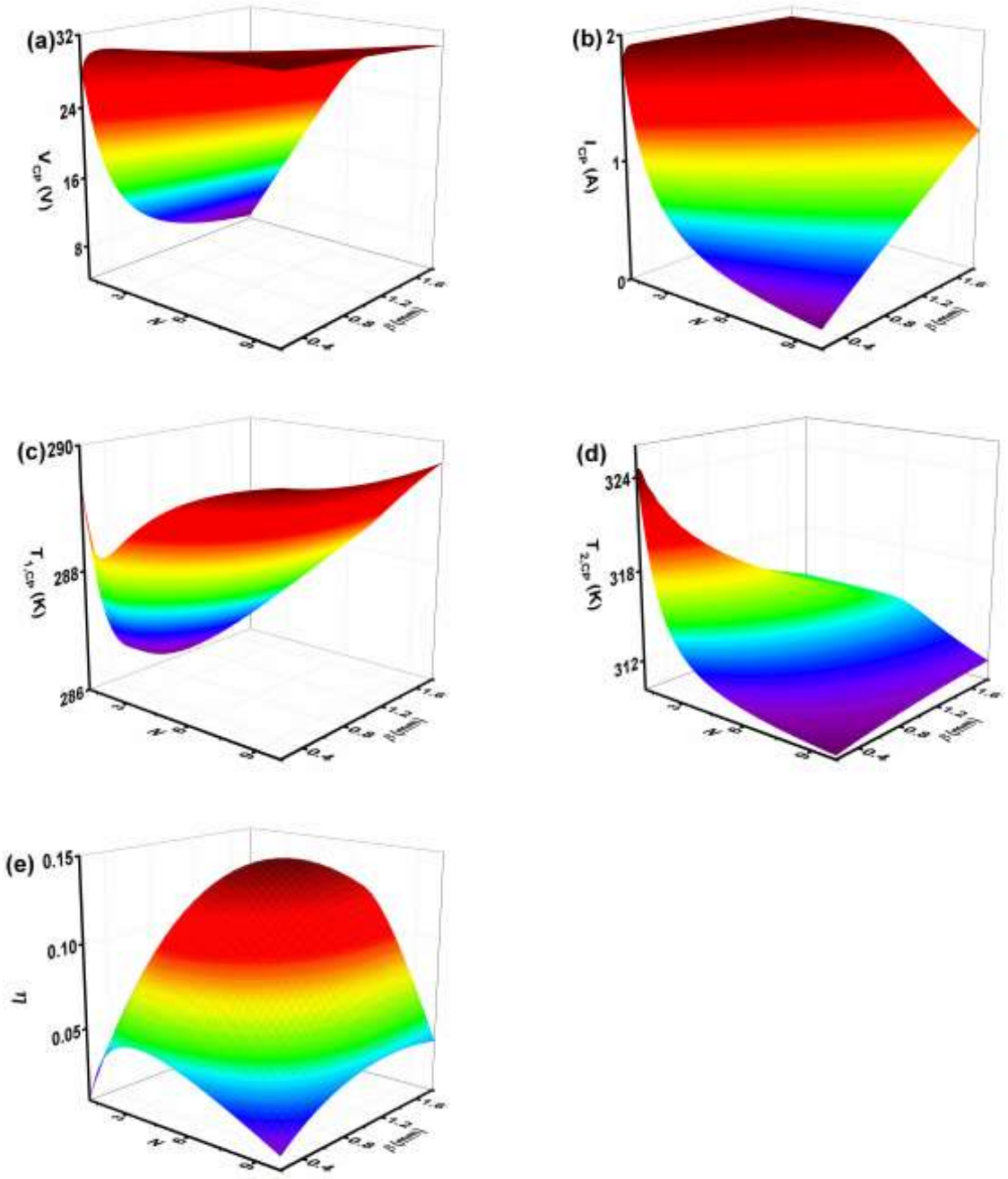

Fig. 3. The 3-D graphs of (a) the coupling voltage V_{CP}, (b) the coupling current I_{CP}, (c) the cold-side's coupling temperature $T_{1,\mathrm{CP}}$, (d) the hot-side's coupling temperature $T_{2,\mathrm{CP}}$, and (e) the energy conversion efficiency η varying with N and β, where the related parameters are same as Fig. 2.

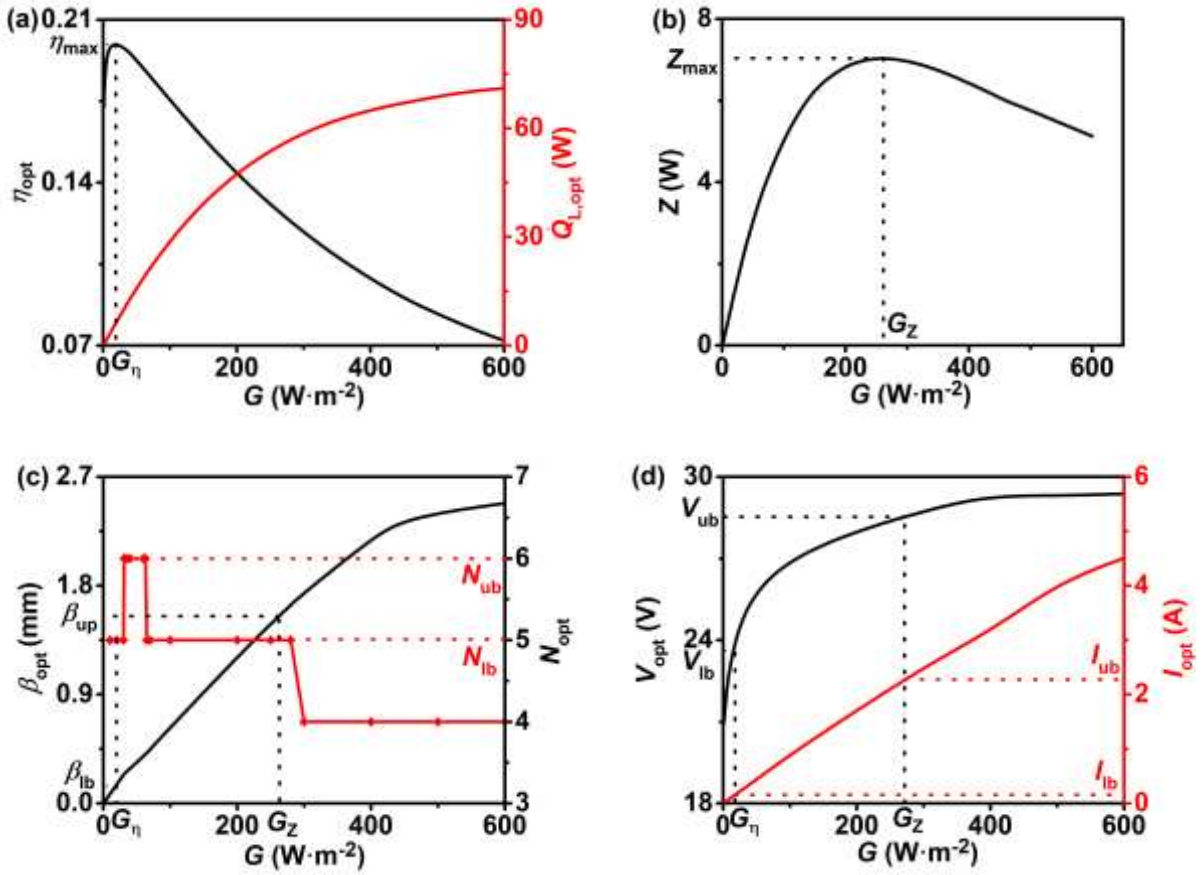

Fig. 4. (a) The optimal efficiency η_{opt} and cooling heat flow rate $\dot{Q}_{\text{L,opt}}$, (b) the objective function $Z = \eta_{\text{opt}} \times \dot{Q}_{\text{L,opt}}$, (c) the optimal structure parameter β_{opt} and TERs number N_{opt}, and (d) the optimal voltage V_{opt} and electrical current I_{opt} as a function of the solar irradiance G, where the related parameters are same as Fig. 2.

Table 1. The effects of the diode ideal factor m on the system's performances.

m	$\eta_{\max}$	$Z_{\max}$ (W)	G_Z $(\mathrm{W}\cdot\mathrm{m}^{-2})$	G_η $(\mathrm{W}\cdot\mathrm{m}^{-2})$	V_{lb} (V)	V_{ub} (V)	I_{lb} (A)	I_{ub} (A)	β_{lb} (mm)	β_{ub} (mm)
1.0	20.0%	7.03	259	18.1	24.5	28.5	0.165	2.22	0.123	1.53
1.5	30.2%	15.9	275	19.8	37.3	42.7	0.178	2.39	0.142	1.53
2.0	40.3%	28.6	265	19.9	49.9	57.5	0.179	2.27	0.147	1.56

Table 2. The effects of the temperature T_{H} on the system's performances, where $m=1$ is chosen.

T_{H} (K)	$\eta_{\max}$	$Z_{\max}$ (W)	G_Z $(\mathrm{W\cdot m^{-2}})$	G_η $(\mathrm{W\cdot m^{-2}})$	V_{lb} (V)	V_{ub} (V)	I_{lb} (A)	I_{ub} (A)	β_{lb} (mm)	β_{ub} (mm)
310	20.0%	7.03	259	18.1	24.5	28.5	0.165	2.22	0.123	1.53
305	28.1%	11.9	249	16.4	24.6	28.4	0.148	2.15	0.154	1.76
300	43.6%	22.6	201	12.3	24.1	28.4	0.111	2.10	0.165	1.72

Table 3. Systems' performance comparisons under the conditions of PV panel's ideal and actual equivalent circuits.

R_s (Ω)	R_{sh} (Ω)	η_{max}	Z_{max} (W)	G_Z $(W \cdot m^{-2})$	G_η $(W \cdot m^{-2})$	V_{lb} (V)	V_{ub} (V)	I_{lb} (A)	I_{ub} (A)	β_{lb} (mm)	β_{ub} (mm)
0.01	10^4	19.9%	6.39	230	17.3	24.3	27.4	0.157	1.95	0.118	1.40
0	∞	20.0%	7.03	259	18.1	24.5	28.5	0.165	2.22	0.123	1.53